2011 IEEE/RSJ International Conference on
Intelligent Robots and Systems
September 25-30, 2011. San Francisco, CA, USA

Trajectory Prediction of Spinning Ball for Ping-Pong Player Robot

Yanlong Huang, De Xu, Min Tan, and Hu Su

Abstract—**An analytic flying model that can well represent the physical behavior is derived, where the ball's self-rotational velocity changes along with the flying velocity. Based on the least square method, a rebound model that represents the relation between the velocities before and after rebound is established. The initial trajectory is fitted to three second order polynomials of the flying time with the measured positions of the ball. The initial velocities of the ball in the analytic flying model, including the flying velocity and the self-rotational velocity, are computed from the polynomials. The ball's landing position and velocity is predicted with the model. The velocities after rebound are determined with the rebound model. By taking the velocities after rebound as new initial ones, the flying trajectory after rebound is described with the model again. In other words, the ball's trajectory is predicted. Experimental results verify the effectiveness of the proposed method.**

Index Terms—**Trajectory prediction, spinning ball, flying modeling, rebounding modeling, least square method, ping-pong player robot.**

I. Introduction

OVER the past few years, the ping-pong robotic system has received much attention [1]-[8]. Anderson [1] designed a ping-pong player robot, which used the robotic arm PUMA 260. Acosta *et al*. [2] built a low-cost ping-pong player robot. Only one camera was used to detect the ball. Moreover, the expert module was applied. Zhang *et al*. [3] designed a 5-degree of freedom (DOF) ping-pong player robot, in which a distributed parallel processing vision system was developed. There was a computer that received the ball's image coordinates from two cameras through the local area network and calculated its 3-dimension (3-D) position online in the reference frame. Matsushima *et al*. [4]-[6] designed a 4-DOF ping-pong player robot and proposed a learning method that consisted of three input-output maps. The method could control the paddle to return the ball to a desired landing point with a specified flight time. Mulling *et al*. [7], [8] designed a 7-DOF ping-pong robotic arm that could mimics human striking behavior.

Trajectory prediction for the flying ball is one of the key techniques in a ping-pong robotic system. The prediction results affect the performance of the robot greatly. It is well known that the Magnus effect on a sphere arises due to spin, the Magnus force that perpendicular to the ball's spin axis and its flying direction will cause the ball to change its flying direction. So the Magnus effect should be considered sufficiently for predicting the trajectory of the spinning ball. Trajectory prediction of non-spinning ball was studied in [3], in this case, the Magnus effect was neglected. The rebound model was also discussed therein, although the rotational velocity was not mentioned therein, the relation of the flying velocities just before and after the rebound could be seen as a compromise between the spinning and non-spinning cases, because the flying velocities used for computing the relative parameters were measured under both conditions. Nonomura *et al*. [9] studied the influence of the Magnus force assuming that the rotational velocity was measured and calculated.

The difficulty in studying the Magus effect is the measurement of the rotational velocity, because it seems that the rotational velocity has nothing to do with the flying velocity and the position. Nakashima *et al*. [10] provided a method of detecting the rotational velocity and derived an analytical model that represented the relation between the flying and the self-rotational velocities of the ball just before and after the rebound. The ball was marked with some feature points. These points were recognized in the image through image processing, then the rotational velocity was calculated. A marked ball was also used for measuring the rotational velocity in [11]. High speed multiple cameras with the capturing rate 900 frames per second (FPS) [10] or 1200 FPS [11] are needed to capture the image of the ball with marks. Tian [12] studied the detection of the rotational velocity through the flight trajectory. The rotational velocity during the flight was supposed to be constant in the reference frame, which meant the spin axis would not change. However, according to the experience and observation, it can be concluded that the spin axis will always be changing during the entire flight.

In this paper, we attempt to model the ball's flying trajectory and estimate its self-rotational velocity. In our model, the ball's self-rotational velocity changes along with its flying velocity in the reference frame. A rebound model based on the least square method (LSM) is proposed, where the flying and self-rotational velocities just before and after the rebound are both considered.

The rest of this paper is organized as follows. Section II proposes the flying model of the spinning ping-pong ball. In section III, the rebound model between the velocities just before and after rebound is discussed. In section IV, the entire trajectory prediction is described. In section V, the experiments are provided to verify the effectiveness of the proposed method. Finally, a conclusion is given in section VI.

This work was supported in part by the National Natural Science Foundation of China under Grant 61075035, and the National High Technology Research and Development Program of China under Grant 2008AA042601.

The authors are with the State Key Laboratory of Intelligent Control and Management of Complex Systems, Institute of Automation, Chinese Academy of Sciences, Beijing 100190, China. (Email: yanlongtu@163.com)

II. THE FLYING MODEL OF PING-PONG BALL

When the spinning ping-pong ball is traveling in the air, it is understandable that the spin axis will change along with its flying velocity. In this section, a dynamic frame {B} is assigned on the ball, as shown in Fig. 1. The axis Y_b is parallel to the flying direction and towards to the opponent side of the robot. The axis X_b is parallel to the table plane and towards right side of the robot. It is sure that the ball's rotational velocity can be treated as a constant in the frame {B}. The reference frame {R} is assigned at some place on the table. The axes Y_r and X_r are parallel to the table sides, and Y_r is from the robot to human.

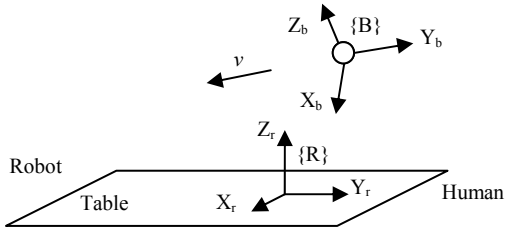

Fig. 1. The reference and the ball frames

Denote the flying velocity of the ball in the frame {R} as $v=\begin{bmatrix} v_x & v_y & v_z \end{bmatrix}^T$. For the unit vector of axis Y_b in the frame {B}, it is written as (1) in the reference {R}.

$$ {}^{r}Y_b = v\,\mathrm{sgn}(v_y)/\|v\| \tag{1}$$

where $\|v\|=\sqrt{v_x^2+v_y^2+v_z^2}$, $\mathrm{sgn}(\cdot)$ is a function with the definition as follows:

$$ \mathrm{sgn}(x)=\begin{cases} 1 & x>0 \\ 0 & x=0 \\ -1 & x<0 \end{cases} \tag{2}$$

Similarly, the unit vectors of axes Y_b and Z_b in the frame {B} can be expressed in the reference {R} as follows:

$$ {}^{r}X_b = \begin{bmatrix} \dfrac{\mathrm{sgn}(v_y)v_y}{v_{xy}} & \dfrac{-\mathrm{sgn}(v_y)v_x}{v_{xy}} & 0 \end{bmatrix}^T \tag{3}$$

$$ {}^{r}Z_b = \begin{bmatrix} \dfrac{-v_x v_z}{\|v\|v_{xy}} & \dfrac{-v_y v_z}{\|v\|v_{xy}} & \dfrac{v_{xy}}{\|v\|} \end{bmatrix}^T \tag{4}$$

where $v_{xy}=\sqrt{v_x^2+v_y^2}$, then the rotation matrix is obtained:

$$ {}^{r}_{b}R = \begin{bmatrix} \dfrac{\mathrm{sgn}(v_y)v_y}{v_{xy}} & \dfrac{\mathrm{sgn}(v_y)v_x}{\|v\|} & \dfrac{-v_x v_z}{\|v\|v_{xy}} \\ \dfrac{-\mathrm{sgn}(v_y)v_x}{v_{xy}} & \dfrac{\mathrm{sgn}(v_y)v_y}{\|v\|} & \dfrac{-v_y v_z}{\|v\|v_{xy}} \\ 0 & \dfrac{\mathrm{sgn}(v_y)v_z}{\|v\|} & \dfrac{v_{xy}}{\|v\|} \end{bmatrix} \tag{5}$$

Denote the self-rotational velocity of the ball in the frame {B} as ${}^{b}\omega=\begin{bmatrix} {}^{b}\omega_x & {}^{b}\omega_y & {}^{b}\omega_z \end{bmatrix}^T$. Using the rotational matrix, the ball's rotational velocity ${}^{r}\omega$ in the frame {R} is obtained:

$$ \begin{aligned} {}^{r}\omega &= {}^{r}_{b}R\,{}^{b}\omega \\ &= \begin{pmatrix} \dfrac{\mathrm{sgn}(v_y)v_y}{v_{xy}}{}^{b}\omega_x + \dfrac{\mathrm{sgn}(v_y)v_x}{\|v\|}{}^{b}\omega_y - \dfrac{v_x v_z}{\|v\|v_{xy}}{}^{b}\omega_z \\ \dfrac{-\mathrm{sgn}(v_y)v_x}{v_{xy}}{}^{b}\omega_x + \dfrac{\mathrm{sgn}(v_y)v_y}{\|v\|}{}^{b}\omega_y - \dfrac{v_y v_z}{\|v\|v_{xy}}{}^{b}\omega_z \\ \dfrac{\mathrm{sgn}(v_y)v_z}{\|v\|}{}^{b}\omega_y + \dfrac{v_{xy}}{\|v\|}{}^{b}\omega_z \end{pmatrix} \end{aligned} \tag{6}$$

While in the air, the flying ball is subject to a net force given by the formula:

$$ F = F_g + F_D + F_M \tag{7}$$

where F_g, F_D and F_M represent the gravitational, drag and Magnus forces, respectively.

In the frame {R}, F_g, F_D and F_M are given by [14], [15]:

$$ F_g = \begin{pmatrix} 0 & 0 & -mg \end{pmatrix}^T \tag{8}$$

$$ F_D = -\frac{1}{2}C_D\rho A\|v\|v \tag{9}$$

$$ F_M = \frac{1}{2}C_M\rho A r\left\|{}^{r}\omega\right\|\|v\|\frac{{}^{r}\omega\times v}{\left\|{}^{r}\omega\times v\right\|} \tag{10}$$

where m is the mass of the ball, g is the acceleration due to gravity, C_D is the drag coefficient, ρ is the density of air, A is the ball's cross-sectional area, C_M is the Magnus coefficient and r is the ball's radius.

The term ${}^{r}\omega\times v$ can be calculated as

$$ {}^{r}\omega\times v = \begin{pmatrix} -\mathrm{sgn}(v_y)\dfrac{v_x v_z}{v_{xy}}{}^{b}\omega_x - \dfrac{v_y\|v\|}{v_{xy}}{}^{b}\omega_z \\ -\mathrm{sgn}(v_y)\dfrac{v_y v_z}{v_{xy}}{}^{b}\omega_x + \dfrac{v_x\|v\|}{v_{xy}}{}^{b}\omega_z \\ \mathrm{sgn}(v_y)v_{xy}{}^{b}\omega_x \end{pmatrix} \tag{11}$$

$$ \left\|{}^{r}\omega\times v\right\| = \sqrt{({}^{r}\omega\times v)^T({}^{r}\omega\times v)} = {}^{b}\omega_{xz}\|v\| \tag{12}$$

where ${}^{b}\omega_{xz}=\sqrt{{}^{b}\omega_x^2+{}^{b}\omega_z^2}$.

From (11) and (12), we have

$$ \frac{{}^{r}\omega\times v}{\left\|{}^{r}\omega\times v\right\|} = \begin{pmatrix} -\mathrm{sgn}(v_y)\dfrac{v_x v_z}{v_{xy}\|v\|}\dfrac{{}^{b}\omega_x}{{}^{b}\omega_{xz}} - \dfrac{v_y}{v_{xy}}\dfrac{{}^{b}\omega_z}{{}^{b}\omega_{xz}} \\ -\mathrm{sgn}(v_y)\dfrac{v_y v_z}{v_{xy}\|v\|}\dfrac{{}^{b}\omega_x}{{}^{b}\omega_{xz}} + \dfrac{v_x}{v_{xy}}\dfrac{{}^{b}\omega_z}{{}^{b}\omega_{xz}} \\ \mathrm{sgn}(v_y)\dfrac{v_{xy}}{\|v\|}\dfrac{{}^{b}\omega_x}{{}^{b}\omega_{xz}} \end{pmatrix} \tag{13}$$

Noticing (6) and taking the properties of rotational matrix into consideration, we have

$$\left\|{}^{r}\omega\right\| = \sqrt{({}^{r}_{b}R\,{}^{b}\omega)^{T}({}^{r}_{b}R\,{}^{b}\omega)} = \sqrt{{}^{b}\omega^{T}\,{}^{b}\omega} = \left\|{}^{b}\omega\right\| \tag{14}$$

Based on the above discussion, an analytical model is derived from (8), (9), (10), (13) and (14).

$$\begin{pmatrix} m\dot{v}_x \\ m\dot{v}_y \\ m\dot{v}_z \end{pmatrix} = \begin{pmatrix} -\frac{1}{2}C_D\rho A\|v\|v_x + \frac{1}{2}C_M\rho Ar\left\|{}^{b}\omega\right\|\|v\|\delta_1 \\ -\frac{1}{2}C_D\rho A\|v\|v_y + \frac{1}{2}C_M\rho Ar\left\|{}^{b}\omega\right\|\|v\|\delta_2 \\ -mg - \frac{1}{2}C_D\rho A\|v\|v_z + \frac{1}{2}C_M\rho Ar\left\|{}^{b}\omega\right\|\|v\|\delta_3 \end{pmatrix} \tag{15}$$

where $\delta_1 = -\mathrm{sgn}(v_y)\dfrac{v_x v_z}{v_{xy}\|v\|}\dfrac{{}^{b}\omega_x}{{}^{b}\omega_{xz}} - \dfrac{v_y}{v_{xy}}\dfrac{{}^{b}\omega_z}{{}^{b}\omega_{xz}}$,

$\delta_2 = -\mathrm{sgn}(v_y)\dfrac{v_y v_z}{v_{xy}\|v\|}\dfrac{{}^{b}\omega_x}{{}^{b}\omega_{xz}} + \dfrac{v_x}{v_{xy}}\dfrac{{}^{b}\omega_z}{{}^{b}\omega_{xz}}$, $\delta_3 = \mathrm{sgn}(v_y)\dfrac{v_{xy}}{\|v\|}\dfrac{{}^{b}\omega_x}{{}^{b}\omega_{xz}}$.

The discrete form of (15) is

$$\begin{pmatrix} x(k+1) \\ y(k+1) \\ z(k+1) \\ v_x(k+1) \\ v_y(k+1) \\ v_z(k+1) \end{pmatrix} = \begin{pmatrix} x(k) \\ y(k) \\ z(k) \\ v_x(k) \\ v_y(k) \\ v_z(k) \end{pmatrix} + \begin{pmatrix} v_x(k) \\ v_y(k) \\ v_z(k) \\ -k_d\|v(k)\|v_x(k) + k_m\left\|{}^{b}\omega\right\|\|v(k)\|\delta_1(k) \\ -k_d\|v(k)\|v_y(k) + k_m\left\|{}^{b}\omega\right\|\|v(k)\|\delta_2(k) \\ -g - k_d\|v(k)\|v_z(k) + k_m\left\|{}^{b}\omega\right\|\|v(k)\|\delta_3(k) \end{pmatrix} T_s \tag{16}$$

where $k_d = \dfrac{C_D\rho A}{2m}$; $k_m = \dfrac{C_M\rho Ar}{2m}$; T_s is sampling period; $x(k)$, $y(k)$ and $z(k)$ are the ball's position in the frame {R} at k-th sampling; $v(k)=[v_x(k)\ \ v_y(k)\ \ v_z(k)]^{\mathrm{T}}$ is the ball's flying velocity at k-th sampling.

Until now, a flying model has been derived, but the rotational velocity is still unknown. From the last three equations in (16), we have

$$\begin{bmatrix} v_x(k+1) - v_x(k) + k_d\|v(k)\|v_x(k)T_s \\ v_y(k+1) - v_y(k) + k_d\|v(k)\|v_y(k)T_s \\ v_z(k+1) - v_z(k) + gT_s + k_d\|v(k)\|v_z(k)T_s \end{bmatrix} = \begin{bmatrix} -\mathrm{sgn}(v_y(k))k_m\dfrac{v_x(k)v_z(k)}{v_{xy}(k)}T_s & -k_m\|v(k)\|\dfrac{v_y(k)}{v_{xy}(k)}T_s \\ -\mathrm{sgn}(v_y(k))k_m\dfrac{v_y(k)v_z(k)}{v_{xy}(k)}T_s & k_m\|v(k)\|\dfrac{v_x(k)}{v_{xy}(k)}T_s \\ \mathrm{sgn}(v_y(k))k_m v_{xy}(k)T_s & 0 \end{bmatrix} \begin{bmatrix} \left\|{}^{b}\omega\right\|\dfrac{{}^{b}\omega_x}{{}^{b}\omega_{xz}} \\ \left\|{}^{b}\omega\right\|\dfrac{{}^{b}\omega_z}{{}^{b}\omega_{xz}} \end{bmatrix} \tag{17}$$

If $v_x(k)$, $v_y(k)$, $v_z(k)$ and $v_x(k+1)$, $v_y(k+1)$, $v_z(k+1)$ in (17) are available, $\left\|{}^{b}\omega\right\|\dfrac{{}^{b}\omega_x}{{}^{b}\omega_{xz}}$ and $\left\|{}^{b}\omega\right\|\dfrac{{}^{b}\omega_z}{{}^{b}\omega_{xz}}$ can be obtained through least square method (LSM).

Supposing that a series of coordinates $x(t)$, $y(t)$ and $z(t)$ is measured. To fit polynomials to the measured data, we have

$$\begin{cases} x(t) = a_1 t^n + a_2 t^{n-1} + \ldots + a_n t + a_{n+1} \\ y(t) = b_1 t^n + b_2 t^{n-1} + \ldots + b_n t + b_{n+1} \\ z(t) = c_1 t^n + c_2 t^{n-1} + \ldots + c_n t + c_{n+1} \end{cases} \tag{18}$$

where a_i, b_i and c_i, i=1,2…n, are the polynomial coefficients. Then the velocities are obtained:

$$\begin{cases} v_x(t) = a_1 n t^{n-1} + a_2(n-1)t^{n-2} + \ldots + a_n \\ v_y(t) = b_1 n t^{n-1} + b_2(n-1)t^{n-2} + \ldots + b_n \\ v_z(t) = c_1 n t^{n-1} + c_2(n-1)t^{n-2} + \ldots + c_n \end{cases} \tag{19}$$

With the velocities in different sampling moments obtained from (19), $\left\|{}^{b}\omega\right\|\dfrac{{}^{b}\omega_x}{{}^{b}\omega_{xz}}$ and $\left\|{}^{b}\omega\right\|\dfrac{{}^{b}\omega_z}{{}^{b}\omega_{xz}}$ are calculated from (17), then $\left\|{}^{b}\omega\right\|$ and $\dfrac{{}^{b}\omega_x}{{}^{b}\omega_z}$ are obtained:

$$\left\|{}^{b}\omega\right\| = \sqrt{(\left\|{}^{b}\omega\right\|\frac{{}^{b}\omega_x}{{}^{b}\omega_{xz}})^2 + (\left\|{}^{b}\omega\right\|\frac{{}^{b}\omega_z}{{}^{b}\omega_{xz}})^2} \tag{20}$$

$$\frac{{}^{b}\omega_x}{{}^{b}\omega_z} = \sqrt{\left(\frac{{}^{b}\omega_{xz}}{{}^{b}\omega_z}\right)^2 - 1} \tag{21}$$

Observe (7), (8), (9) and (10), it can be found that

$$(F/m - F_g/m - F_D/m)^{T}\,{}^{r}\omega = 0 \tag{22}$$

From (5) and (6), (22) is rewritten in the expanded form

$$\begin{pmatrix} \dot{v}_x + \frac{1}{2m}C_D\rho A\|v\|v_x \\ \dot{v}_y + \frac{1}{2m}C_D\rho A\|v\|v_y \\ \dot{v}_z + g + \frac{1}{2m}C_D\rho A\|v\|v_z \end{pmatrix}^{T} \left(\begin{bmatrix} \dfrac{\mathrm{sgn}(v_y)v_y}{v_{xy}} & \dfrac{\mathrm{sgn}(v_y)v_x}{\|v\|} & \dfrac{-v_x v_z}{\|v\|v_{xy}} \\ \dfrac{-\mathrm{sgn}(v_y)v_x}{v_{xy}} & \dfrac{\mathrm{sgn}(v_y)v_y}{\|v\|} & \dfrac{-v_y v_z}{\|v\|v_{xy}} \\ 0 & \dfrac{\mathrm{sgn}(v_y)v_z}{\|v\|} & \dfrac{v_{xy}}{\|v\|} \end{bmatrix} \begin{bmatrix} {}^{b}\omega_x \\ {}^{b}\omega_y \\ {}^{b}\omega_z \end{bmatrix} \right) = 0 \tag{23}$$

The discrete form of (23) is

$$\begin{pmatrix} v_x(k+1) - v_x(k) + k_d\|v(k)\|v_x(k)T_s \\ v_y(k+1) - v_y(k) + k_d\|v(k)\|v_y(k)T_s \\ v_z(k+1) - v_z(k) + gT_s + k_d\|v(k)\|v_z(k)T_s \end{pmatrix}^{T} *$$

$$\left(\begin{bmatrix} \dfrac{\mathrm{sgn}(v_y(k))v_y(k)}{v_{xy}(k)} & \dfrac{\mathrm{sgn}(v_y(k))v_x(k)}{\|v(k)\|} & \dfrac{-v_x(k)v_z(k)}{\|v(k)\|v_{xy}(k)} \\ \dfrac{-\mathrm{sgn}(v_y(k))v_x(k)}{v_{xy}(k)} & \dfrac{\mathrm{sgn}(v_y(k))v_y(k)}{\|v(k)\|} & \dfrac{-v_y(k)v_z(k)}{\|v(k)\|v_{xy}(k)} \\ 0 & \dfrac{\mathrm{sgn}(v_y(k))v_z(k)}{\|v(k)\|} & \dfrac{v_{xy}(k)}{\|v(k)\|} \end{bmatrix} \begin{bmatrix} {}^{b}\omega_x \\ {}^{b}\omega_y \\ {}^{b}\omega_z \end{bmatrix} \right) = 0 \tag{24}$$

Denote ${}^{r}_{b}R = \{R_{ij}\}$, i, j=1, 2, 3,

$$\begin{cases} m_1 = v_x(k+1) - v_x(k) + k_d\|v(k)\|v_x(k)T_s \\ m_2 = v_y(k+1) - v_y(k) + k_d\|v(k)\|v_y(k)T_s \\ m_3 = v_z(k+1) - v_z(k) + gT_s + k_d\|v(k)\|v_z(k)T_s \\ n_1 = m_1 R_{11}(k) + m_2 R_{21}(k) + m_3 R_{31}(k) \\ n_2 = m_1 R_{12}(k) + m_2 R_{22}(k) + m_3 R_{32}(k) \\ n_3 = m_1 R_{13}(k) + m_2 R_{23}(k) + m_3 R_{33}(k) \end{cases} \tag{25}$$

$$\begin{cases} e_1 = \dfrac{{}^b\omega_x}{{}^b\omega_z} \\ e_2 = \dfrac{{}^b\omega_y}{{}^b\omega_z} = (-n_3 - n_1 e_1)/n_2 \\ e_3 = 1 \\ e = [e_1 \quad e_2 \quad e_3]^T \end{cases} \tag{26}$$

$${}^b\omega_e = e / \|e\| \operatorname{sgn}({}^b\omega_z / {}^b\omega_{xz}) \tag{27}$$

From (20), (21) and (24), it can be proved that

$${}^b\omega = \left[{}^b\omega_x \quad {}^b\omega_y \quad {}^b\omega_z \right]^T = \left\| {}^b\omega \right\| {}^b\omega_e \tag{28}$$

III. The Rebound Model Between Ball and Table

In this section, the rebound model between the spinning ball and the table is discussed. The model represents the relation between the flying and self-rotational velocities (v_{xout} , v_{yout} , v_{zout} , ${}^b\omega_{xout}$, ${}^b\omega_{yout}$, ${}^b\omega_{zout}$) just after rebound and the velocities (v_{xin} , v_{yin} , v_{zin} , ${}^b\omega_{xin}$, ${}^b\omega_{yin}$, ${}^b\omega_{zin}$) just before rebound.

Take the physical properties corresponding to the rebound phenomenon into consideration, the rebound model is described as

$$\begin{cases} v_{xout} = [v_{xin} \quad \omega_{yin} \quad 1] b_1 \\ v_{yout} = [v_{yin} \quad \omega_{xin} \quad 1] b_2 \\ v_{zout} = [v_{zin} \quad 1] b_3 \\ \omega_{xout} = [v_{yin} \quad \omega_{xin} \quad 1] b_4 \\ \omega_{yout} = [v_{xin} \quad \omega_{yin} \quad 1] b_5 \\ \omega_{zout} = [\omega_{zin} \quad 1] b_6 \end{cases} \tag{29}$$

where $b_i \in R^3, i = 1,2,4,5$, $b_j \in R^2, i = 3,6$.

Fitting several measured positions before rebound, a group of the flying and self-rotational velocities just before rebound are calculated with (17), (19), (20), (21), (27) and (28). Similarly, a group of velocities just after rebound are calculated through fitting several measured positions after rebound. Once the velocities in (29) have been computed, the parameters b_i are obtained with the LSM.

After the rebound parameters b_i are completed, the output velocities (v_{xout} , v_{yout} , v_{zout} , ${}^b\omega_{xout}$, ${}^b\omega_{yout}$, ${}^b\omega_{zout}$) just after rebound are calculated using (29) when the new input velocities (v_{xin} , v_{yin} , v_{zin} , ${}^b\omega_{xin}$, ${}^b\omega_{yin}$, ${}^b\omega_{zin}$) just before rebound are given.

IV. The Trajectory Prediction

In section II and III, we have discussed the flying model of ping-pong ball and the rebound model between ball and table. In this section, the entire procedure of trajectory prediction is described in the following steps.

Step 1: A series of measured positions are needed from the ball's flying trajectory, which can be obtained using the stereo vision system. These positions are treated as the initial trajectory and select one position from it as the initial one.

Step 2: Fitting three second order polynomials to the initial trajectory using (18), then the initial flying velocity is calculated using (19). According to (17), (19), (20), (21), (27) and (28), initial self-rotational velocity is obtained using two flying velocities in adjacent sampling moments.

Step 3: Predict the ball's flying trajectory from the initial state using (16). Once $z(k)$ reaches the ball's radius, the ball lands on the table. The position $x(k)$, $y(k)$ and $z(k)$ at this moment is called landing position and the flying velocity just before rebound is computed.

Step 4: According to (29), the velocities including the flying velocity and the self-rotational velocity just after rebound are calculated as new initial ones. The prediction proceeds with (16) again.

Step 5: Select a striking position from the predicted trajectory after rebound, this point is used for striking the ping-pong ball by the robot player.

V. Experiments and Results

In this experiment, a distributed parallel processing stereo vision system was used, which could measure the 3-D positions of the flying ball online.

Before the prediction, several entire trajectories were measured, then the velocities just before and after rebound in (29) were computed. The rebound parameters were estimated with LSM as follows

b_1 =[0.6278 -0.0003 -0.0344]^T, b_2 =[0.7796 0.0011 0.3273]^T

b_3 =[-0.5498 0.8735]^T, b_4 =[7.4760 0.1205 39.4228]^T

b_5 =[-22.9295 0.1838 -13.4791]^T, b_6 =[-0.3270 39.9528]^T

The other relative experiment parameters were given as follows

m=0.0027kg, g=9.802m/s^2, C_D=0.5, C_M=1, r=0.02m, A=0.0013m^2, ρ=1.29kg/m^3, T_s=1ms.

A series of experiments was conducted to compare the proposed method with the method in [3], in which the ball was with heavy self-rotation. In experiments, the ball's positions on the flying trajectory were continuously measured in order to assess the predicted results with the proposed method and the method in [3]. In the prediction procedure, only the first several measured positions of the ball's trajectory were used, they were used to fit initial trajectory. The sequent trajectory in each experiment was predicted with the proposed method and the method in [3]. The results of the flying and self-rotational velocities just before and after the rebound predicted with the proposed method were listed in Table I, while the flying velocities predicted by the method in [3] were listed in Table II. It can be found that the velocities just before and after the rebound predicted with the proposed method are coincide with the results with the method in [3], the self-rotational velocities can be given by the proposed method. Here, the actual self-rotational velocities were not known since the ball was struck by the human opponent. But the estimated velocities could be verified by comparing the predicted trajectories with actual ones. It means that if the predicted trajectories coincided well with the actual ones, the velocities were estimated properly. The landing and striking

positions errors were calculated next, these results reflected the precision of the predicted velocities to some extent.

TABLE I
FLYING AND ROTATIONAL VELOCITIES PREDICTED WITH THE PROPOSED METHOD

No	(v_{xin}, v_{yin}, v_{zin}) m/s	(ω_{xin} , ω_{yin}, ω_{zin}) rad/s	(v_{xout}, v_{yout}, v_{zout}) m/s	(ω_{xout},ω_{yout},ω_{zout}) rad/s
1	0.92, -2.89, -2.46	-39.85, -9.21, 1.91	0.54, -1.97, 2.22	12.98, -36.19, 39.33
2	-0.20, -3.03, -2.57	-43.34, -28.42, 29.87	-0.15, -2.08, 2.28	11.53, -14.09, 30.19
3	0.45, -3.21, -2.60	27.78, -25.26, 0.07	0.26, -2.14, 2.31	18.77, -28.45, 39.93
4	0.72, -2.96, -2.61	52.33, 20.46, 0.64	0.41, -1.92, 2.31	23.61, -26.29, 39.74
5	0.41, -3.14, -2.64	-23.19, -38.59, 79.71	0.24, -2.14, 2.32	13.17, -30.16, 13.89
6	0.29, -2.70, -2.50	-38.07, -28.61, 32.62	0.16, -1.82, 2.25	14.67, -25.46, 29.29
7	-0.27, -2.71, -2.59	-32.26, -41.99, 32.28	-0.19, -1.82, 2.30	15.24, -15.12, 29.40
8	-0.41, -3.04, -2.86	-45.19, -13.47, 10.97	-0.29, -2.09, 2.45	11.24, -6.52, 36.37
9	-0.46, -2.64, -2.98	-45.89, -18.06, 53.94	-0.32, -1.78, 2.51	14.19, -6.19, 22.31
10	-0.24, -3.07, -2.62	-43.32, -29.35, 1.41	-0.18, -2.11, 2.31	11.28, -13.34, 39.49
11	-0.52, -3.18, -2.68	-19.41, -55.60, 9.88	-0.35, -2.17, 2.35	13.29, -11.73, 36.72
12	-0.35, -3.17, -2.64	-52.17, -0.19, 24.67	-0.25, -2.20, 2.32	9.47, -5.48, 31.89

TABLE II
FLYING VELOCITIES PREDICTED WITH THE METHOD IN [3]

No	(v_{xin}, v_{yin}, v_{zin}) m/s	(v_{xout}, v_{yout}, v_{zout}) m/s
1	0.66, -2.96, -2.45	0.45, -1.92, 2.20
2	-0.39, -3.06, -2.49	-0.23, -1.98, 2.23
3	0.23, -3.23, -2.61	0.17, -2.09, 2.31
4	0.38, -3.02, -2.62	0.27, -1.95, 2.32
5	0.34,-3.27, -2.44	0.24, -2.11, 2.20
6	0.22, -2.74, -2.46	0.17, -1.77, 2.21
7	-0.41, -2.76, -2.51	-0.24, -1.78, 2.25
8	-0.67, -3.02, -2.83	-0.41, -1.95, 2.47
9	-0.62, -2.70, -2.88	-0.37, -1.74, 2.51
10	-0.40, -3.05, -2.62	-0.24, -1.97, 2.32
11	-0.76, -3.18, -2.61	-0.46, -2.05, 2.32
12	-0.54, -3.18, -2.58	-0.32, -2.05, 2.30

Because the ball's radius was 20 mm, the landing position in z-direction was 20 mm. The striking position in z-direction was defined to be 250 mm. Fig. 2(a) shows the measured landing positions and the landing positions predicted with the proposed method and the method in [3] in X-Y plane. Fig. 2(b) shows the errors of the landing positions predicted with the two methods. The error was the distance between the predicted and the measured positions. Fig. 2(c) shows the measured striking positions and the striking positions predicted with the proposed method and the method in [3] in X-Y plane. Fig. 2(d) shows the errors of the striking positions predicted with the different methods. It can be seen from Fig. 2(b) and 2(d), the proposed method performs much better than the method in [3]. For the method in [3], the errors of the landing positions are small, because the self-rotational velocity affects the flying trajectory slightly. After the rebound, the errors of the striking positions are large. As known, the flying velocity changes rapidly just after rebound due to the ball's self-rotational velocity. If the rotational velocity is not considered sufficiently, the predicted trajectory after rebound will largely deviate from the actual one.

The actual trajectory and predicted trajectories in experiments are given in Fig. 3. In Fig. 3(a) and 3(b), the maximum errors of the trajectory predicted with the method in [3] were (-117.32, 8.42, -28.88) mm and (56.55, 5.36, 19.25) mm respectively, while the errors of the trajectory predicted with the proposed method were (7.90, 6.56, -46.28) mm and (1.51, -15.13, 5.29) mm. The direction of self-rotation velocity that mainly affect the trajectory in Fig. 3(a) was opposite to the one in Fig. 3(b), thus, one trajectory appeared right deviation while the other one was left deviation.

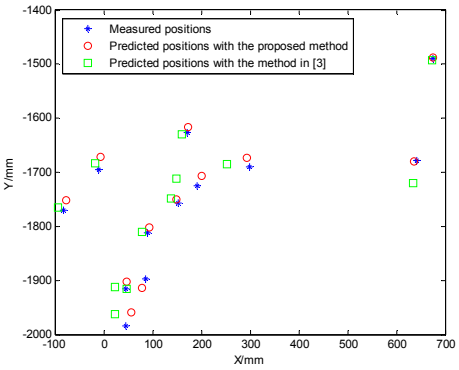

(a)

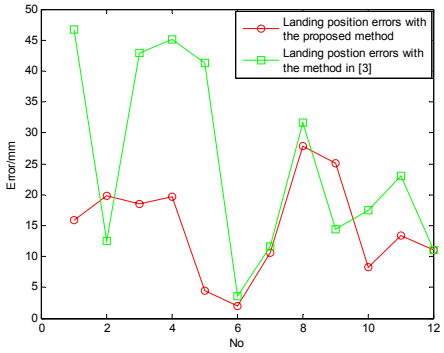

(b)

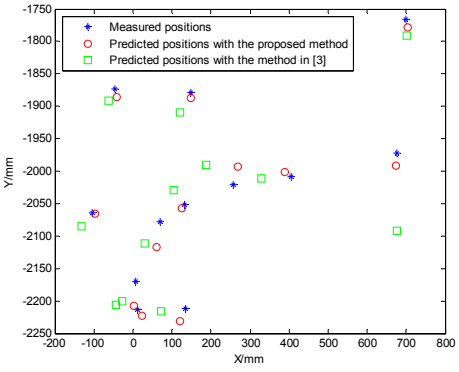

(c)

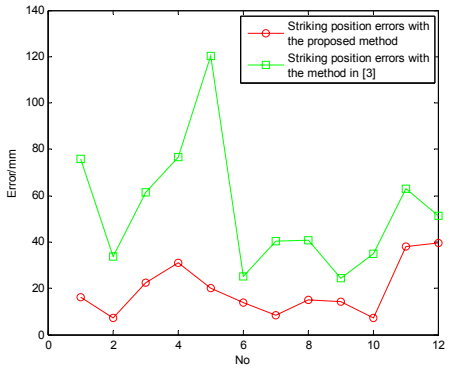

(d)

Fig. 2. Landing and striking positions. (a) Landing positions. (b) Errors of the landing positions. (c) Striking positions. (d) Errors of the striking positions.

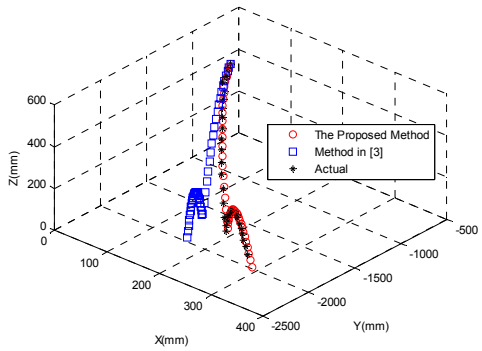

(a)

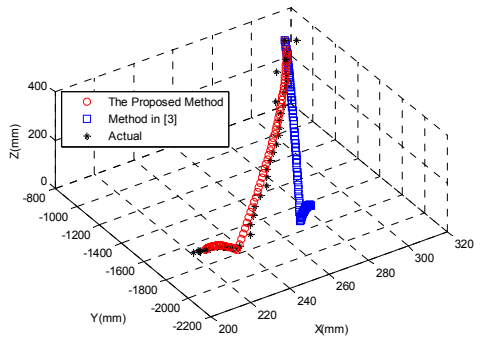

(b)

Fig. 3. Actual trajectory and predicted trajectories. (a) First trajectory comparison. (b) Second trajectory comparison.

Due to the error of initial velocity computed from the (19), the flying velocity and self-rotational velocity are not quite accurate, the errors of landing and striking positions are unavoidable. More measured positions used for fitting the polynomial in (18) will be useful for improving the precision. Moreover, the measured positions are affected by several factors such as the camera calibration.

VI. Conclusions

An analytic flying model that can well represent the physical behavior is proposed. The ball's self-rotational velocity is estimated from its flying trajectory. The rebound model is established using LSM, where a linear relation between the flying and self-rotational velocities just before and after rebound is implemented. The entire procedure of trajectory prediction is described in detail. Experiment shows the effectiveness of the proposed method, the prediction of landing position and striking position performs satisfactorily.

References

[1] R. L. Anderson, *A Robot Ping-Pong Player: Experiments in Real Time Control*. Cambridge, MA: MIT Press, 1987.

[2] L. Acosta, J. J. Rodrigo, J. A. Mendez, G. N. Marichal, and M. Sigut, "Ping-pong player prototype," *IEEE Robotics & Automation Magazine*, vol. 10, no.4, pp. 44-52, 2003.

[3] Z. Zhang, D. Xu, and M. Tan, "Visual measurement and prediction of ball trajectory for table tennis robot," *IEEE Transactions on Instrumentation and Measurement*, vol. 59, no. 12, pp. 3195-3205, 2010.

[4] M. Matsushima, T. Hashimoto, M. Takeuchi, and F. Miyazaki, "A learning approach to robotic table tennis robotics," *IEEE Transactions on Robotics and Automation*, vol. 21, no. 4, pp. 767-771, 2005.

[5] M. Matsushima, T. Hashimoto, and F. Miyazaki, "Learning to the robot table tennis task-ball control & rally with a human," in *Proc. IEEE Int. Conf. on Systems, Man and Cybernetics*, Washington D.C., USA, 2003, pp. 2962-2969.

[6] F. Miyazaki, M. Matsushima, and M. Takeuchi, "Learning to dynamically manipulate: a table tennis robot controls a ball and rallies with a human being," *Advances in Robot Control*, Springer, 2006.

[7] K. Mulling, J. Kober, and J. Peters, "Simulating human table tennis with a biomimetic robot setup," *Lecture Notes in Computer Science*, Springer, 2010.

[8] K. Mulling and J. Peters, "A computational model of human table tennis for robot application," *Autonome Mobile Systeme*, 2009.

[9] J. Nonomura, A. Nakashima, and Y. Hayakawa, "Analysis of effects of rebounds and aerodynamics for trajectory of table tennis ball," in *Proc. SICE Annual Conference*, Taipei, Taiwan, 2010, pp.1567-1572.

[10] A. Nakashima, Y. Ogawa, Y. Kobayashi, and Y. Hayakawa, "Modeling of rebound phenomenon of a rigid ball with friction and elastic effects," in *Proc. American Control Conference*, Baltimore, MD, USA, 2010, pp.1410-1415.

[11] S. Furuno, K. Kobayashi, T. Okubo, and Y. Kurihara, "A study on spin-rate measurement using a uniquely marked moving ball," in *Proc. ICROS-SICE International Joint Conference*, Japan, 2009, pp.3439-3442.

[12] Y. Tian, *High-speed Moving Object Identification Prediction And Operation Planning For Humanoid Robots*. PhD thesis, Beijing institute of technology, Beijing, China, 2010.

[13] S. Schaal and C. G. Atkeson," Robot juggling: an implementation of memory-based learning," *IEEE Control Systems Magazine*, vol. 14, no.1, pp. 57-71, Feb, 1994.

[14] B. G. Cook and J. E. Goff , "Parameter space for successful soccer kicks," *European Journal of Physics*, vol. 27, pp. 865-874, 2006.

[15] R. K. Adir, "The physics of baseball," *Physics Today*, pp. 26-31, May, 1995.